In Situ Structural Changes upon Electrochemical Lithium Insertion in Nanosized Anatase TiO_2

U. Lafont,*,† D. Carta,‡,§ G. Mountjoy,‡ A. V. Chadwick,‡ and E. M. Kelder†

NanoStructured Materials, Delft.Chem.Tech., TU Delft, Julianalaan 136, 2628 BL Delft, The Netherlands, Functional Materials Group, School of Physical Sciences, University of Kent, Canterbury, Kent, CT2 7NR, U.K., and Dipartimento di Scienze Chimiche, Università di Cagliari, SS 554 bivio per Sestu, Monserrato, 09042 Cagliari, Italy

Received: September 11, 2009; Revised Manuscript Received: December 9, 2009

The intercalation of lithium in nanosized TiO_2 has been studied for its application as an electrode for rechargeable Li-ion batteries. In this paper, we use a synthesis process in order to obtain a low-density anatase TiO_2 presenting monocrystalline particles of 7−8 nm. These textural characteristics allow this material to host almost twice as much Li (300 $mAh \cdot g^{-1}$) than that of a micrometer sized anatase. In this study, in situ X-ray absorption spectroscopy is used to monitor and understand the structural changes that happen upon lithium insertion/removal, leading to a reversible two-phase transition process: TiO_2 ($I4_1/amd$) → Li-titanate (*Imma*) → Li_1TiO_2 ($I4_1/amd$).

Introduction

Materials with a controlled texture are suitable to enhance the interactions between the material itself and an external medium (liquid, gas, or even solid). TiO_2 can accept lithium in its structure and can be used as an electrode material in Li-ion batteries. In this respect, the TiO_2 polymorphs anatase ($I4_1/amd$), rutile[1–5] ($P4_2/mnm$), brookite[4] (*Pbca*), TiO_2[B][1,6] ("bronze", $C2/m$), TiO_2[R][7–9] ("ramsdellite", *Pbnm*), TiO_2[H][10] ("hollandite", $I4/m$), and amorphous,[11] have been studied in order to investigate their behavior upon lithium insertion/removal. In addition, nanostructured TiO_2 will exhibit better lithium ion transfer due to a better electrolyte/material interaction compared with the bulk nonporous material and shorter diffusion paths in the solid.

Whittingham et al.[12] were the first to investigate chemical insertion of lithium in anatase TiO_2 using *n*-butyllithium. From this study, it appears that a composition of $Li_{0.6}TiO_2$ can be reached in the anatase TiO_2. In 1979, Ozhuku et al.[13] performed electrochemical insertion of lithium using 1 M $LiClO_4$ in propylene carbonate as electrolyte: the insertion mechanism shows a phase transition exhibiting a plateau at 1.78 V versus Li/Li^+. Since then, different studies using Raman, NMR, X-ray absorption spectroscopy, and X-ray and neutron diffraction have been performed to understand the behavior upon Li insertion/removal in anatase TiO_2. To monitor the structural evolution of the anatase phase versus the amount of inserted lithium, ex situ measurements were performed. For this purpose, Li_xTiO_2 samples were used where x is tuned using chemical lithiation by *n*-butyllithium. This reagent is known to mimic a potentiostatic electrochemical Li insertion at 1 V versus Li/Li^+; therefore, it can be expected to insert lithium to a great extent. However, it needs to be stressed that chemical (CLi) and electrochemical (ELi) lithiation in galvanostatic mode seem to differ in the maximum amount of lithium that can be inserted.[1]

Bonino et al.[14] showed by ex situ XRD on ELi anatase TiO_2 the existence of a new phase for $Li_{0.6}TiO_2$ that was not in agreement with the presence of the cubic $LiTiO_2$ phase[13] claimed earlier. Indeed, using a CLi anatase TiO_2 sample and neutron diffraction, Cava et al.[15] reported that the tetragonal anatase TiO_2 phase ($I4_1/amd$) undergoes a phase transition to an orthorhombic $Li_{0.5}TiO_2$ phase (Li-titanate *Imma*). Using ex-situ XRD on ELi anatase,[16] this reversible phase transition upon Li insertion/removal has been confirmed. Moreover, with a fast progress in synthesis processes for the formation of nanosized material, new trends appear: Li intercalation into anatase TiO_2 presents a different behavior, depending on the size of the crystallite domains.[17,18] In that regard, it has been suggested recently in a neutron diffraction study using CLi that, at room temperature, nanosized anatase TiO_2 can accept extra lithium in the structure, leading to a new phase transition to Li_1TiO_2. This new phase shows the same space group as that of the anatase phase ($I4_1/amd$), but with shifted lattice parameters a and c that change from 3.792 to 4.043 Å and from 9.497 to 8.628 Å, respectively.[18] Moreover, calculation or ex situ measurements on the CLi sample have recently shown for TiO_2[R][19] and rutile,[5] respectively, that titanates can exhibit Li_1TiO_2 as new phases. The stability and existence of Li_1TiO_2 are strongly related to the material's texture (e.g., nanosized). It is clear that nanosized and/or porous anatase materials present increased capacity upon cycling compared with bulk micrometer sized anatase.[20–28] However, to our knowledge, none of the earlier studies made on ELi anatase[1,13,14,16,22–35] show any suggestions or evidence of the Li_1TiO_2 phase corresponding to a theoretical capacity of 335 $mAh \cdot g^{-1}$. Obviously, this new obtained phase is quite interesting with regard to its theoretical capacity of 335 $mAh \cdot g^{-1}$.

On the one hand, electrochemical lithiation and performance of anatase as an electrode are extensively studied and are important with regard to direct applications. On the other hand, clarification of the insertion mechanisms in micrometer sized and nanosized anatase in terms of structural refinement, Li diffusion, Li bonding, Li population, and Ti oxidation state have been performed using mainly ex situ measurements on chemi-

* To whom correspondence should be addressed. E-mail: u.lafont@tudelft.nl (U.L.), e.m.kelder@tudelft.nl (E.M.K.).
† TU Delft.
‡ University of Kent.
§ Università di Cagliari.

10.1021/jp908786t
Published on Web 12/22/2009

cally lithiated anatase samples. With technical progress, in situ experiments can be carried out (in situ XAS, Raman, XRD, and UV) and can bridge the gap between fundamental and practical studies.

In this work, we will focus on the structural changes that occur during the electrochemical insertion/removal of lithium in nanocrystalline anatase TiO_2 monitored by in situ X-ray absorption near-edge structure (XANES) and extended X-ray absorption fine structure (EXAFS).

Experimental Section

The mesoporous nanosized TiO_2 materials have been synthesized using a modified sol−gel method, as previously reported.[36] However, in brief, titanium isopropoxide (Aldrich) is mixed with glycol ether (2-butoxyethanol BCS, Aldrich). The resulting solution is dropped into a water/surfactant (nonionic triblock copolymer P123, Aldrich) mixture. The resulting pale yellow and dense solution is stirred for 24 h, followed by aging without stirring at room temperature for another 24 h. The molar ratio of the solution is Ti/BCS/H_2O/surfactant = 1:12:42:0.01. The TiO_2 powder is recovered by filtration and washed with ethanol and deionized water. To remove the organic compounds still present and to obtain the required mesoporosity, the as-synthesized material undergoes a thermal treatment under an air flow at 350 °C for 8 h. Transmission electron microscopy (TEM) was performed using a Philips CM30T electron microscope with a LaB_6 filament as electron source operated at 300 kV. For these measurements, ground samples were mounted on Quantifoil carbon polymer microgrid supported on a copper grid. X-ray diffraction data were recorded using Cu Kα (λ = 1.54056 Å) radiation on a Bruker D8 ADVANCE X-ray diffractometer.

The working electrodes were prepared by grinding in a mortar TiO_2 material, carbon black (99.9%, <1 μm, Alfa Aesar) and polyvinylidene fluoride (PVDF, Solvay) as binder. Some drops of 1-methyl-2-pyrrolidone (NMP, Merks-Schuchardt) were added in order to obtain a homogeneous paste. The final paste composition is 80% active material, 10% carbon, and 10% binder in weight. This paste was deposited on an aluminum strip with a 200 μm thick doctor blade and immediately dried at 80 °C for a couple of hours. The aluminum-coated strip was then laminated until it reached a thickness of 70 μm. The electrochemical tests were performed using CR2320 coin cells (Hohsen) using 1 M $LiPF_6$ in EC/DMC (2:1) (Mitsubishi Chemical) as electrolyte and metallic lithium as negative electrode. The coin cells were sealed in a He-filled glovebox (H_2O < 5 ppm). During the charge−discharge tests, the coin cells were kept under pressure with Hoffman clamps to ensure good electrical contacts. The samples were tested in galvanostatic mode using a MACCOR S4000 tester.

In situ XANES and EXAFS measurements at the Ti K-edge were carried out on station 7.1 at the SRS at Daresbury Laboratory, U.K. The measurements were performed in normal transmission mode using a Si(111) monochromator and gas-filled ion chambers. A third ion chamber was used to collect the XAS of a Ti foil placed after the signal ion chamber. This provided a reference for the calibration of the Ti K-edge position for each scan. The energy scales were calibrated taking as the reference the Ti K-edge of Ti metal. For this purpose, "coffee-bag" cells have been built following the plastic Li-ion cell procedure developed by Bellcore.[37] The cells were cycled on a MACCOR S2000 tester, and the XAS spectra were recorded at different states of discharge/charge. EXAFS data analysis was performed using the program Viper[38] to obtain the normalized absorbance χ as a function of the modulus of the photoelectron wave vector k, and the modular package DL_EXCURV,[39] based on the EXCURV98 code, was used in the final stage of data processing to model the experimental $k^3\chi(k)$ in order to extract structural information.

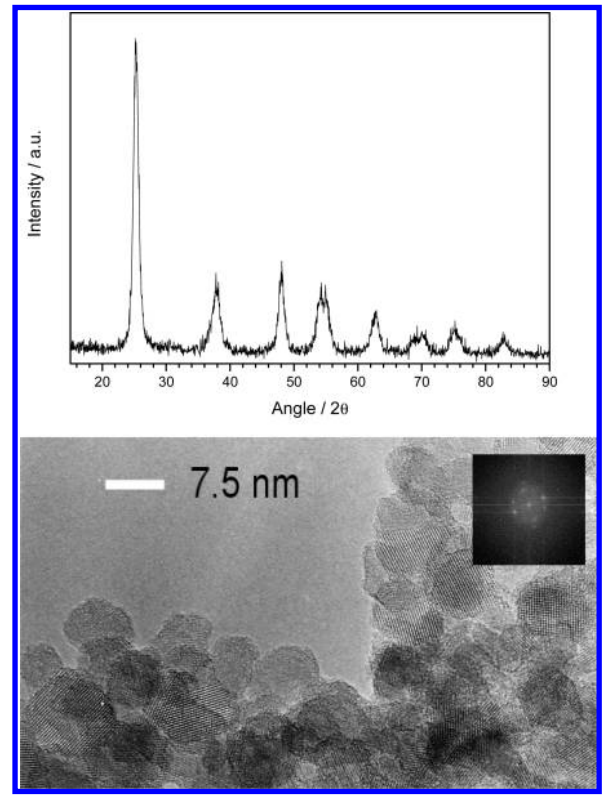

Figure 1. (Top) XRD pattern of nano TiO_2 anatase material. (Bottom) HRTEM image showing the spherical monocrystalline particles (the diffraction pattern of a single particle is shown as the inset).

Results and Discussion

Synthesis. The synthesis procedure was targeted to form highly divided anatase TiO_2 particles presenting interesting textural characteristics, such as high surface area and small particles. This nanostructure has been confirmed by XRD and TEM, as we can see in Figure 1. The XRD pattern clearly shows that this TiO_2 material presents the TiO_2 anatase phase. Using the Scherrer formula, the calculated crystallite size is about 8 nm. We can see in the HRTEM images that this TiO_2 material is made of homogeneous nanocrystallites of 7−8 nm. This material shows monocrystalline nanoparticles. Textural investigations based on N_2 adsorption−desorption have been previously reported showing a high surface area and a sharp pore-size distribution in the range of mesopores.[36] Indeed, the isotherm curves present a real type IV isotherm with an H2-type hysteresis. The material exhibits a surface area of 200 $m^2 \cdot g^{-1}$, according to the BET calculation, a porous volume of 0.22 $mL \cdot g^{-1}$, and a pore size of 4.6 nm (mesopores), according to the Broekhoff and De Boer (BdB) pore calculation model.

Electrochemical Testing. Figure 2 shows the electrochemical test performed in galvanostatic mode using a current of 15 $mA \cdot g^{-1}$ between 2.5 and 0.8 V. The discharge profile can be divided in 3 regions: (A) before a constant voltage plateau (V > 1.76 V), (B) the constant voltage plateau (1.76 > V>1.74 V), and (C) after the constant voltage plateau (V < 1.74 V). During discharge in region (A), the voltage quickly decreases, giving a composition of $Li_{0.1}TiO_2$ (33 $mAh \cdot g^{-1}$). Region (B) shows a

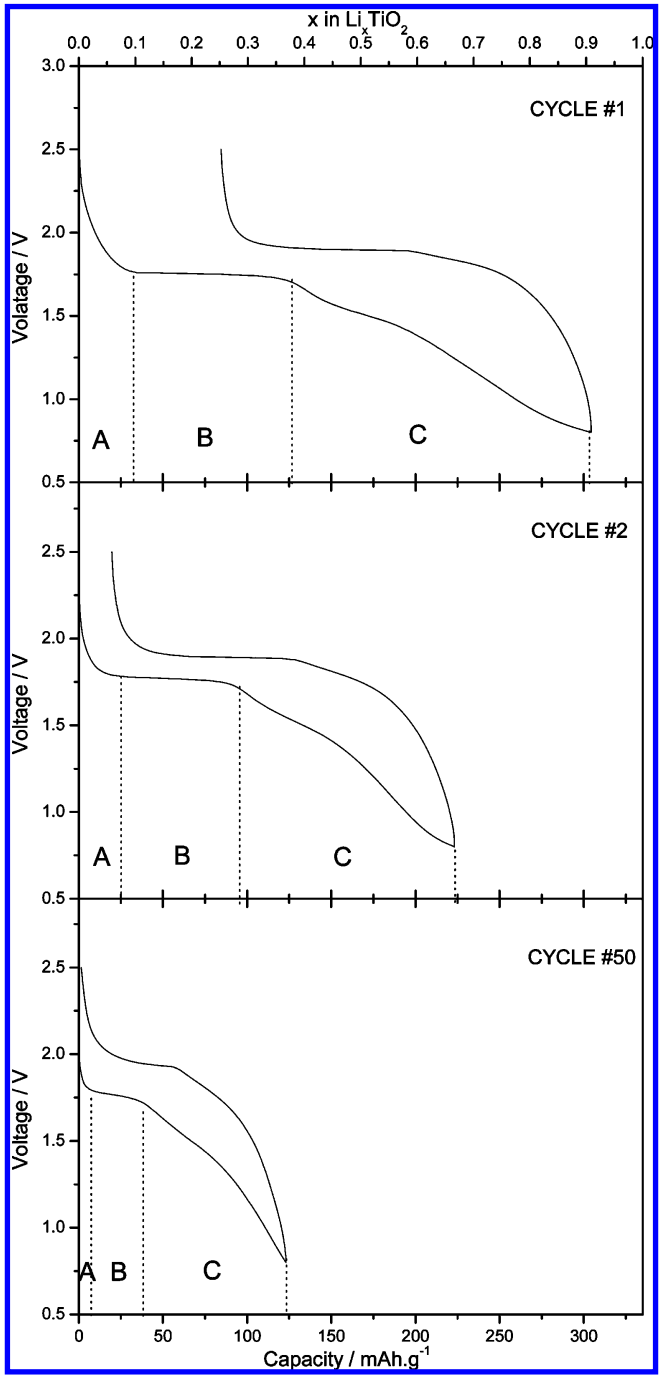

Figure 2. Galvanostatic cycling curves of nano TiO_2 at 15 mA·g^{-1} between 2.5 and 0.8 V.

plateau that is attributed to the presence of a well-known biphasic domain. After this well-defined plateau, the potential is slowly going down. The aim of this study is to understand the phenomena leading to region (C). The existence of this intercalation domain has to be related to either a second biphasic domain or an extended solid-solution-like behavior. However, at the end of the first discharge, the material reaches a composition of $Li_{0.9}TiO_2$, which represents a capacity of 300 mAh·g^{-1}. During the lithium removal (charge), the three regions can be clearly distinguish with the main plateau at 1.9 V. During the second cycle, the discharge/charge curves present the same profile, but with a reduction of the capacity. This obtained capacity fading occurs in every region. These capacities for each of the regions, derived from the discharge/charge curves, are gathered in Figure 3. After 50 cycles, the capacity that can be

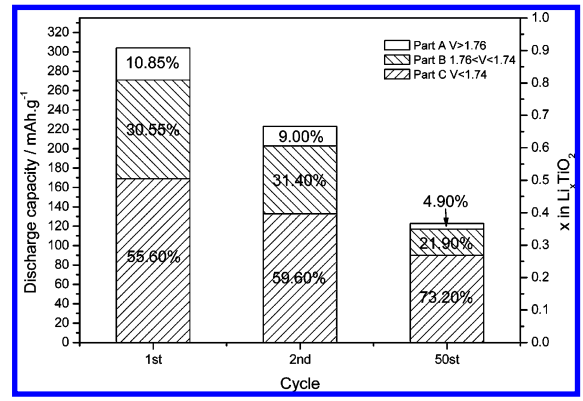

Figure 3. Discharge capacity proportions for each characteristic region of the insertion process as a function of cycle life.

attributed to the discharge and charge plateau are very low, 27 and 29 mAh·g^{-1}, respectively.

The Li insertion process in region (A) is attributed to the formation of a solid solution. This implies the insertion of Li ions into the anatase structure without any phase transition, hence, leading to a Li-poor titanate phase denoted as $Li_\varepsilon TiO_2$, presenting the same space group as the anatase TiO_2 phase, namely, $I4_1/amd$. From the electrochemical measurements, the nano TiO_2 material is then able to reach a composition of $Li_{0.1}TiO_2$ without any structural changes. This value is in agreement with the data already published for Li insertion in nanosized anatase showing an extension of the solid solution domain compared to micrometer sized anatase.[18,23,25] Nevertheless, this result confirms that nanosized crystals can accept more Li atoms without any changes from a structural point of view. Upon lithiation, the capacity related to this Li-poor phase decreases (Figure 3), becoming negligible after 50 cycles. This solid solution is strongly dependent to the surface state of the particles and is obviously related to irreversible surface phenomena (SEI) during the first cycles. The voltage profile in region (B), that is, the constant voltage plateau, corresponds to the well-known biphasic domain[14,15] in which a phase transitions occurs between the $Li_\varepsilon TiO_2$ and the Li-titanate phase ($Li_{0.5}TiO_2$ *Imma*). It is interesting to note the evolution of the capacities related to this part. During the first cycle, this capacity represents 33% of the total capacity, after the second cycle 31%, and after the 50th cycle, 22% only. After this biphasic domain, the voltage decreases down to 1.5 V where a second pseudoplateau can be distinguish. Indeed, a second voltage plateau has already been observed[1,29] earlier by inserting lithium in micrometer sized anatase at 120 °C. However, the phase transition involved was only investigated by neutron diffraction[18] using CLi samples but has never been discussed for ELi samples despite the presence of this pseudoplateau at room temperature in many studies.[22,24–28,35,40] The galvanostatic measurement versus Li/Li$^+$ shows an interesting behavior compared to bulk micrometer sized anatase TiO_2 in which the capacity originating from region (C) is usually extremely low.

In Situ XAS (XANES and EXAFS). During the in situ XAS experiment, the material undergoes 1.5 cycles in galvanostatic mode between 3.0 and 1.0 V with a 15 mA·g^{-1} current. XAS spectra have been recorded at 14 different states of charge/discharge (Figure 4) labeled by letters. The galvanostatic measurement shows an irreversible capacity of 0.2 Li per TiO_2 formula unit during the first cycle. This capacity loss during the first charge is not directly assignable to Li insertion phenomena as it will be discussed further. Due to the high surface area of our material (200 m^2·g^{-1}) and the nanoparticles'

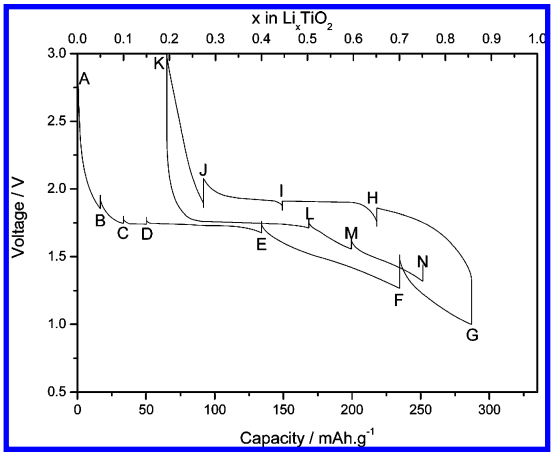

Figure 4. Galvanostatic cycling curves of nano TiO_2 using coffee-bag cells during in situ XAS measurement (at 15 mA·g^{-1} between 3.0 and 1.0 V). Each measurement at a different state of discharge/charge is labeled by a letter.

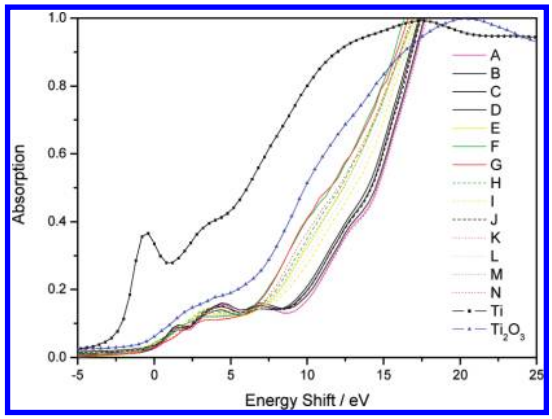

Figure 5. Ti K-edge XANES data recorded at different states of charge/discharge. Ti_2O_3 has been used as reference for the Ti^{3+} oxidation state. The letters at each curve agree with those from Figure 4.

size, all surface and parasitic reactions taking place at the solid/liquid interface are increased. In this respect, we can suspect that these Li-consuming parasitic reactions related to electrolyte, solvent, and presence of impurities are the most plausible explanation for the capacity loss, as it has been already shown for nanosized material.[41]

The in situ XAS measurement presented in Figure 5 shows a shift of the Ti adsorption edge to lower energies upon Li insertion. During the intercalation of the Li ions into the anatase structure, the oxidation state of the Ti atoms is reduced. The in situ XAS measurement presented in Figure 5 shows a shift of the Ti adsorption edge to lower energies upon Li insertion. This shift clearly indicates that the average oxidation state of the Ti atoms is reduced. Figure 6 presents the evolution of the Ti oxidation state as a function of x in Li_xTiO_2, deduced from the first derivative of the edge using Ti_2O_3 as reference for Ti^{3+}. However, we have to keep in mind that the estimate of the valence from XANES is only accurate to 7% at best due to energy calibration (±0.2 eV) of the monochromator during the experiments.

During the discharge, the reduction of Ti^{4+} to Ti^{3+} occurs by inserting lithium. At the end of the discharge, Ti atoms show an oxidation state proportional to the amount of Li inserted. During the charge, Ti atoms are oxidized back to Ti^{4+} and are, therefore, dependent on the Li content. The XANES pre-edge at the Ti K-edge (Figure 7) shows for the pristine material four different peaks. Most of the studies made on the Ti K-pre-edge

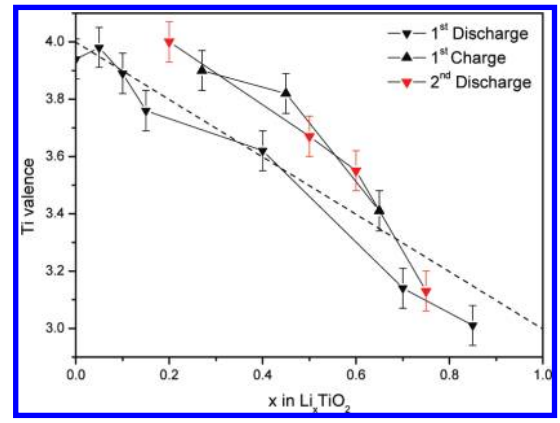

Figure 6. Ti oxidation state variation as a function of Li content during cycling.

region on anatase material[42–45] identified these four peaks as A1, A2, and A3 that correspond to 3d−4p hybridized state transition and B to 4p−4s.[46] In the pristine phase, the A1 peak can be assigned to the surrounding four Ti atoms in the first Ti−Ti shell. A2 and A3 are related to medium range order via the hybridization of the central Ti 4p orbital with the Ti 3d orbitals of the second Ti−Ti shell. A1 is a quadrupolar transition of the t_{2g} state. A2 is dipolar in nature but includes a small e_g quadrupolar component, and A3 is a pure dipolar component.[46] Peak B results from the 4p Ti orbitals hybridized with the near Ti 4s and/or O 2p a_1-type orbitals. Upon lithiation until at points A, B, C, and D during discharge and at J and K during charge, the main features of the pristine material are still present, and thus, the basic anatase structure is maintained. For $Li_{0.4}TiO_2$ in E at the end of the plateau, only one peak can be clearly distinguished at 3.2 eV. This feature is typical when the octahedral coordination of Ti changes from regular to distorted octahedral.[42] It is different from the pristine material, where anatase has regular octahedra (with six Ti−O distances very similar). This feature is attributed to the Li-titanate phase, where octahedra are distorted (with a splitting of the Ti−O shell into three shorter and three longer Ti−O distances). For $Li_{0.7}TiO_2$ (at point F), the intensity of this 3.2 eV peak is weakened, but shoulders appear around 2.0 eV and at 0.4 eV. For $Li_{0.85}TiO_2$ (at point G) and also during lithium removal, the pre-edge feature in H presents the same behavior as at point F (three peaks at 0.4, 2.0, and 3.2 eV). These three peaks compare to the single feature observed for the $Li_{0.4}TiO_2$ composition (E) and can be related to the presence of more regular TiO_6 octahedra. In I, the peaks A1, A3, and B from the pristine material are hardly visible, and the peak at 3.2 eV due to the Li-titanate phase is then dominant, as was seen at E. Upon the second lithiation (points L, M, and N), the evolution of the pre-edge follows the same trend as during the first discharge. During Li insertion, the regular TiO_6 octahedra of the pristine undergo a first distortion and then become more regular for a high Li content. Apart from the change in the shape of the pre-edge peaks, the position of the peaks shifts to lower energy during lithiation, clearly following the change in valence of Ti, which shifts the XANES spectrum to lower energies.

The in situ FTs of the EXAFS spectra are presented in Figure 8. Upon Li intercalation, it is clear that EXAFS radial distribution functions do not exhibit any differences up to a composition of $Li_{0.15}TiO_2$. The pristine structure is maintained in which the Li atoms occupy four-coordinated sites at the center of distorted octahedral holes. For a composition of $Li_{0.4}TiO_2$ (at point E) at the end of the plateau, a structural evolution appears. The

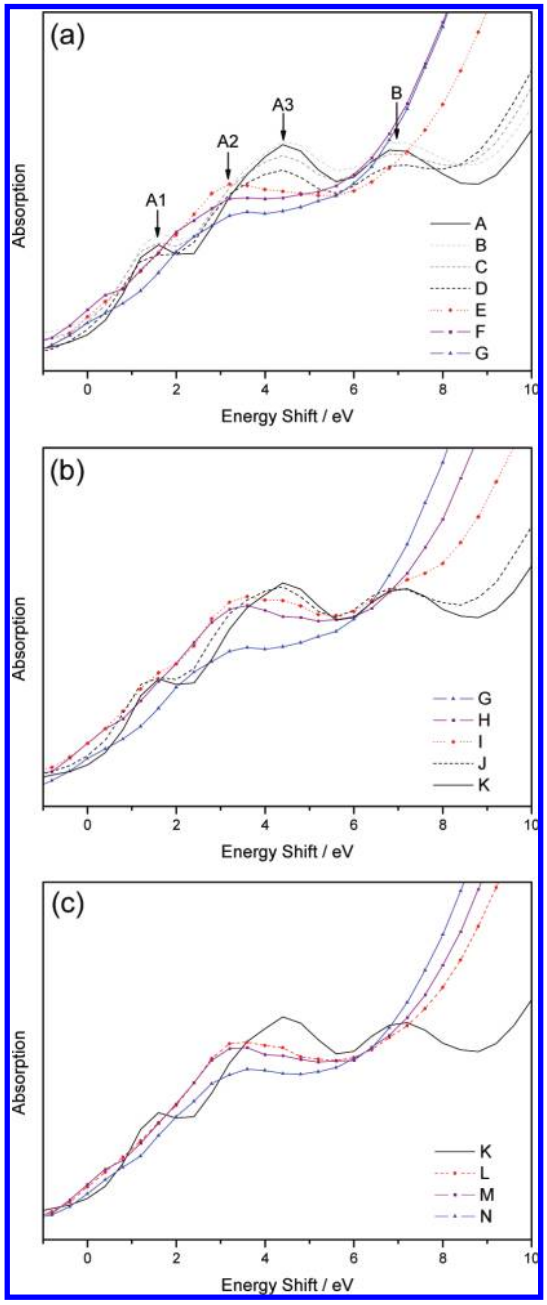

Figure 7. Ti K-edge XANES pre-edge feature during Li insertion/removal for (a) first discharge, (b) first charge, and (c) second discharge. The letters agree with those from Figure 4.

crystalline phase has been refined with the well-known Li-titanate orthorhombic phase $Li_{0.5}TiO_2$ (space group *Imma*). Note that the first coordination shell in pristine anatase has six Ti−O distances close to 1.93 Å, whereas in Li-titanate, the first coordination shell shows a marked splitting. The first subshell has three Ti−O distances all close to 1.93 Å and, hence, a small Debye−Waller (DW) factor, $2\sigma^2$, like that in anatase, whereas the second subshell involves three Ti−O distances over a larger range and, hence, a larger DW factor (see Table 1). For the compositions $Li_{0.7}TiO_2$ (at point F) and $Li_{0.85}TiO_2$ (at point G), the EXAFS data exhibit another structural modification. It was predicted by Koudriachova et al.[47] that a stable $LiTiO_2$ structure must have a full occupation of the central octahedral holes by lithium, then giving it a distorted rock-salt structure. Indeed, this structure has been observed in $LiScO_2$.[48] Using these parameters but with reduced distances (because Ti is smaller than Sc), the $Li_{0.7-0.85}TiO_2$ crystalline structure has been refined,

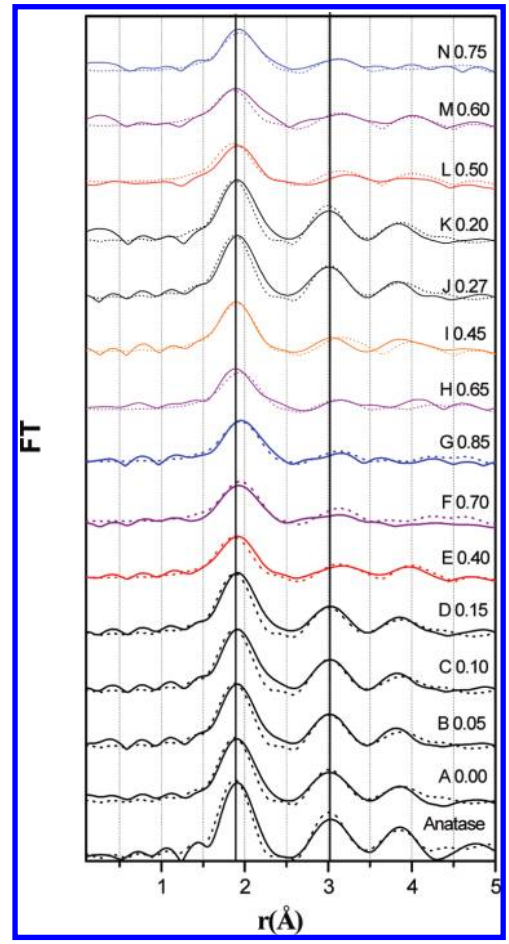

Figure 8. Fitted (dotted line) and experimental (full line) EXAFS FT data recorded at different states of charge/discharge. The letters at each curve agree with those from Figure 4.

TABLE 1: EXAFS Fit Parameters for the Nano TiO_2 Sample at Various Li Contents

sample Li_xTiO_2	shell	R (Å)	N*[a]	$2\sigma^2$ (Å^2)	R_{factor} (%)
$x = 0$ in A	O	1.93(1)	6	0.011(1)	39
TiO_2 $I4_1/amd$	Ti	3.02(1)	4	0.011(1)	
	O	3.82(3)	8	0.006(1)	
	Ti	3.82(3)	4	0.025(2)	
	O	4.30(5)	16	0.040(4)	
	O	4.79(5)	4	0.036(4)	
$x = 0.4$ in E	O	1.93(1)	3	0.010(1)	40
Li-titanate *Imma*	O	2.01(1)	3	0.026(1)	
	Ti	3.12(1)	4	0.025(1)	
	O	3.50(3)	4	0.036(3)	
	O	3.78(3)	4	0.028(3)	
	Ti	3.94(3)	4	0.017(2)	
	O	4.39(5)	8	0.030(3)	
	O	4.67(5)	8	0.018(2)	
$x = 0.70$ in F	O	2.01(1)	6	0.010(1)	40
Li_1TiO_2 $I4_1/amd$	Ti	3.13(1)	4	0.026(1)	
	O	3.80(3)	8	0.025(2)	
	Ti	4.14(3)	4	0.036(4)	
	O	4.70(5)	16	0.028(3)	
	O	4.99(5)	4	0.017(2)	

[a] The values of N were fixed to reduce the number of fitting parameters.

showing the Li_1TiO_2 structure (space group $I4_1/amd$), similar to anatase, but with expanded cell parameters. In the Li_1TiO_2 structure, the first coordination shell has six Ti−O distances at the same length and, hence, a small DW factor like that in anatase. Notice that following the structural transitions, the

EXAFS fitting is done first with one Ti−O shell, then with a split Ti−O shell, then with one Ti−O shell. This is expected because the Ti sites follow the valence, first, being mostly Ti^{4+}, then a mixture of Ti^{4+} and Ti^{3+}, and then being mostly Ti^{3+}. During lithium removal from the structure, these phase transitions are reversible. At points H and M, the material shows again the Li-titanate and Li_1TiO_2 phase, and thus, the EXAFS data are not well-fitted, neither by the pristine phase nor by the Li-titanate phase. This is obvious since, here too, in the material, two phases coexist. After full delithiation, the material recovers the original anatase structure. After the first phase transition, in L and later at point M, the material initiates its second phase transition (Li-titanate to Li_1TiO_2) that ends with the presence of only Li_1TiO_2 at point N. From the in situ measurements, it is clear that the material undergoes a two-phase transition upon lithium insertion. Before the first phase transition, XAS measurements are in agreement with the electrochemical tests and then clearly show that nanocrystalline anatase can host 0.15 Li per TiO_2 formula unit without any structural changes.

This extension of the first solid solution domain for nanosized anatase has already been report as 0.21[18] and 0.22.[23] This effect, which mainly occurs during the first lithium insertion and drastically disappears upon cycling, is related to a capacitive effect[23] induced by a high surface area. The difference between the obtained value here (0.15) and the value reported earlier using anatase nanomaterials presenting the same crystallite size can be explain as follows. Although the surface area of the material and, thus, the particle size, plays an important role in this phenomenon, the termination (referred to as condensation or relaxation) of the surface is the key point. We have to keep in mind that increasing the active surface area of a material will automatically increase the phenomena related to its surface. Indeed, nanomaterials synthesized at low temperature[23] might present a higher degree of uncondensed surface bonds, higher surface defect concentration, and, therefore, a higher amorphous component. Lithium insertion in amorphous TiO_2 presents a solid-solution-like behavior[11] without any phase transition. In this respect, Li interaction with the surface occurs but does not imply structural changes. On the other hand, nanomaterials synthesized using enough energy to well terminate the crystal structure either by longer thermal treatment time or by higher temperature show a less amorphous component and, thus, a smaller solid solution domain.

At 1.75 V versus Li/Li^+, the first phase transition starts at the beginning of the main plateau. At this voltage, a coexistence of nanoparticles of anatase and nanoparticles of the orthorhombic Li-titanate phase ($Li_{0.5}TiO_2$) is obtained. This first phase transition ends at the end of the constant voltage plateau, for instance, at point E. At this step, all the material exhibits the Li-titanate phase in which the Li ions occupied half of the octahedral sites. This is also the case for micrometer sized anatase particles for which a maximum composition of $Li_{0.5-0.6}TiO_2$ can be reached. For nanosized particles, more lithium can be inserted in the material at this step. Indeed, after the first biphasic transition, the electrochemical measurements present a sloppy curve in which a pseudoplateau is present at 1.5 V versus Li/Li^+. This pseudoplateau indicates a second biphasic domain: more lithium is inserted in the structure, as shown by a continuous reduction of Ti oxidation state to +3, and the structure is changing, as shown by the evolution of the Li-titanate EXAFS signature. The $LiTiO_2$ phase present at the end of the discharge implies a full occupation of octahedral site by Li in the structure. The three phase transitions upon Li insertion in nanocrystalline anatase are summarized in Figure 9.

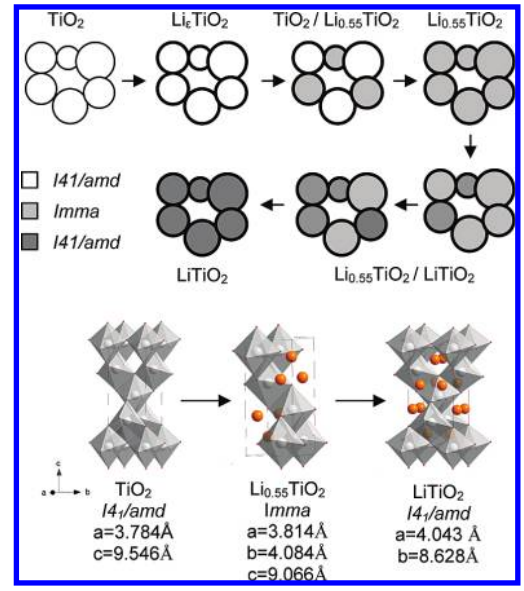

Figure 9. Phase transition upon Li insertion in anatase TiO_2 (gray = Ti, red = O, orange = Li). Cell parameters of $LiTiO_2$ are deduced from ref 18.

The full occupation of the octahedral sites in the $LiTiO_2$ structure implies a change in the unit cell parameter compared with the isomorphic anatase structure. As it can be seen in Table 1, the shells present increased distances compared with the pristine phase. This can be related to an increased *a* parameter and a reduced *c* parameter (Figure 9). The full occupation of the octahedral sites implies also a poor Li ion diffusion within the crystallites. This loss in Li ion mobility as a function of lithium content is well-established by previous studies using CLi anatase samples.[17,18,49] The in situ XAS experiments have been performed during 1.5 cycles, showing fully reversible phase transitions. However, after 50 cycles, the material presents a lower specific capacity and, more generally, a fading of the capacity related to the first phase transition. It looks like less pristine material is then available. This phenomenon can be explained by the formation of an irreversible or kinetically restricted phase. The electrochemical tests performed in galvanostatic mode imply a certain current (15 $mA \cdot g^{-1}$) and, thus, imply the Li ions a certain mobility in the system. Due to the presence of the $LiTiO_2$ phase, the Li mobility is reduced within this phase. During the lithium removal process, not all the $LiTiO_2$ particles can undergo the phase transitions back to the pristine phase. After several cycles, there is an increase in the amount of particles still having the "kinetically irreversible" $LiTiO_2$ phase. After 50 cycles, capacity loss is close to 60% of the initial capacity.

Conclusions

The TiO_2 material, showing a well-defined nanocrystallite size (7−8 nm), reaches the composition of $Li_{0.9}TiO_2$ upon electrochemical lithiation. However, a huge capacity fading due to parasitic reactions occurs during the first charge where 0.2 Li/TiO_2 is not recovered. The pristine anatase phase undergoes two phase transitions: TiO_2 (*I*4_1/*amd*) → Li-titanate (*Imma*) and then Li-titanate (*Imma*) → Li_1TiO_2 (*I*4_1/*amd*). The presence and reversibility of these phase transitions have been well-established by in situ XAS. As was suspected for several years, the use of

nanosized material for energy storage can exhibit new behaviors and good benefits. In our case, the decrease in particle size does not lead to a better Li mobility due to reduced diffusion length, as is always expected in this type of material. The presence of nanoparticles is necessary for the formation of the new $LiTiO_2$ phase showing increased capacity, but the low Li mobility within this new phase due to the full occupation of the octahedral site undermines the benefits of the low diffusion length.

Acknowledgment. The authors would like to thank the ALISTORE benchmarking unit via M. Morcrette for his contribution in plastic battery assembly, M. Wagemaker for useful discussions, and the European Commission for funding via the ALISTORE network of excellence. D. Carta is grateful to the Royal Society for an International Incoming Short Visits 2007/R3 (Grant 21340).

References and Notes

(1) Zachau-Christiansen, B.; West, K.; Jacobsen, T.; Atlung, S. *Solid State Ionics* **1988**, *28*−*30*, 1176.
(2) Kavan, L.; Fattakhova, D.; Krtil, P. *J. Electrochem. Soc.* **1999**, *146*, 1375.
(3) Hu, Y.-S.; Kienle, L.; Guo, Y.-G.; Maier, J. *Adv. Mater.* **2006**, *18*, 1421.
(4) Reddy, M. A.; Kishore, M. S.; Pralong, V.; Varadaraju, U. V.; Raveau, B. *Electrochem. Solid-State Lett.* **2007**, *10*, A29.
(5) Borghols, W. J. H.; Wagemaker, M.; Lafont, U.; Kelder, E. M.; Mulder, F. M. *Chem. Mater.* **2008**, *20*, 2949.
(6) Armstrong, A. R.; Armstrong, G.; Canales, J.; Bruce, P. G. *Angew. Chem., Int. Ed.* **2004**, *43*, 2286.
(7) Gover, R. K. B.; Tolchard, J. R.; Tukamoto, H.; Murai, T.; Irvine, J. T. S. *J. Electrochem. Soc.* **1999**, *146*, 4348.
(8) Kuhn, A.; Amandi, R.; Garcia-Alvarado, F. *J. Power Sources* **2001**, *92*, 221.
(9) Kuhn, A.; Baehtz, C.; Garcia-Alvarado, F. *J. Power Sources* **2007**, *174*, 421.
(10) Noailles, L. D.; Johnson, C. S.; Vaughey, J. T.; Thackeray, M. M. *J. Power Sources* **1999**, *81*−*82*, 259.
(11) Hibino, M.; Abe, K.; Mochizuki, M.; Miyayama, M. *J. Power Sources* **2004**, *126*, 139.
(12) Whittingham, M. S.; Dines, M. B. *J. Electrochem. Soc.* **1977**, *124*, 1387.
(13) Ohzuku, T.; Takehara, Z.; Yoshizawa, S. *Electrochim. Acta* **1979**, *24*, 219.
(14) Bonino, F.; Busani, L.; Lazzari, M.; Manstretta, M.; Scrosati, B. *J. Power Sources* **1981**, *6*, 261.
(15) Cava, R. J.; Murphy, D. W.; Zahurak, S.; Santoro, A.; Roth, R. S. *J. Solid State Chem.* **1984**, *53*, 64.
(16) Ohzuku, T.; Kodama, T. *J. Power Sources* **1985**, *14*, 153.
(17) Wagemaker, M.; Borghols, W. J. H.; van Eck, E. R. H.; Kentgens, A. P. M.; Kearley, G. J.; Mulder, F. M. *Chem.*−*Eur. J.* **2007**, *13*, 2023.
(18) Wagemaker, M.; Borghols, W. J. H.; Mulder, F. M. *J. Am. Chem. Soc.* **2007**, *129*, 4323.
(19) Koudriachova, M. V. *Chem. Phys. Lett.* **2008**, *458*, 108.
(20) Luca, V.; Hanley, T. L.; Roberts, N. K.; Howe, R. F. *Chem. Mater.* **1999**, *11*, 2089.
(21) Kavan, L.; Kalbac, M.; Zukalova, M.; Exnar, I.; Lorenzen, V.; Nesper, R.; Gratzel, M. *Chem. Mater.* **2004**, *16*, 477.
(22) Gao, X.; Zhu, H.; Pan, G.; Ye, S.; Lan, Y.; Wu, F.; Song, D. *J. Phys. Chem. B* **2004**, *108*, 2868.
(23) Sudant, G.; Baudrin, E.; Larcher, D.; Tarascon, J.-M. *J. Mater. Chem.* **2005**, *15*, 1263.
(24) Subramanian, V.; Karki, A.; Gnanasekar, K. I.; Ebby, F. P.; Rambabu, B. *J. Power Sources* **2006**, *159*, 186.
(25) Hardwick, L. J.; Holzapfel, M.; Novak, P.; Dupont, L.; Baudrin, E. *Electrochim. Acta* **2007**, *52*, 5357.
(26) Jiang, C.; Wei, M.; Qi, Z.; Kudo, T.; Honma, I.; Zhou, H. *J. Power Sources* **2007**, *166*, 239.
(27) Wang, Z.; Liu, S.; Chen, G.; Xia, D. *Electrochem. Solid-State Lett.* **2007**, *10*, A77.
(28) Kubiak, P.; Geserick, J.; Husing, N.; Wohlfahrt-Mehrens, M. *J. Power Sources* **2008**, *175*, 510.
(29) Macklin, W. J.; Neat, R. J. *Solid State Ionics* **1992**, *53*−*56*, 694.
(30) Exnar, I.; Kavan, L.; Huang, S. Y.; Gratzel, M. *J. Power Sources* **1997**, *68*, 720.
(31) Kavan, L.; rathousky, J.; Gratzel, M.; Shklover, V.; Zukal, A. *J. Phys. Chem. B* **2000**, *104*, 12012.
(32) Wagemaker, M.; Lutzenkirchen-Hecht, D.; Keil, P.; van Well, A. A.; Frahm, R. *Physica B* **2003**, *336*, 118.
(33) Smirnov, M.; Baddour-Hadjean, R. *J. Chem. Phys.* **2004**, *121*, 2348.
(34) Wilhelm, O.; Pratsinis, S. E.; de Chambrier, E.; Crouzet, M.; Exnar, I. *J. Power Sources* **2004**, *134*, 197.
(35) Yamada, H.; Yamato, T.; Moriguchi, I.; Kudo, T. *Chem. Lett.* **2004**, *33*, 1548.
(36) Lafont, U.; Kooyman, P.; Galarneau, A.; Renzo, F. D. *Stud. Surf. Sci. Catal.* **2005**, *155*, 355.
(37) Tarascon, J.-M.; Gozdz, A. S.; Schmutz, C.; Shokoohi, F.; Warren, P. C. *Solid State Ionics* **1996**, *86*−*88*, 49.
(38) Klementev, K. V. *J. Phys. D: Appl. Phys.* **2001**, *34*, 209.
(39) Tomic, S.; Searle, B. G.; Wander, A.; Harrison, N. M.; Dent, A. J.; Mosselmans, J. F. W.; Inglesfield, J. E. *CCLRC Technical Report DL-TR-2005-001*; CCRLC: Warrington, U.K., 2005; ISSN: .
(40) Xu, J.; Jia, C.; Cao, B.; Zhang, W. F. *Electrochim. Acta* **2007**, *52*, 8044.
(41) Kavan, L.; Prochazka, J.; Spitler, T. M.; Kalbac, M.; Zukalova, M. T.; Drezen, T.; Gratzel, M. *J. Electrochem. Soc.* **2003**, *150*, A1000.
(42) Farges, F.; Brown, G. E.; Rehr, J. J. *Phys. Rev. B* **1997**, *56*, 1809.
(43) Stewart, S. J.; Fernandez-Garcia, M.; Belver, C.; Mun, B. S.; Requejo, F. G. *J. Phys. Chem. B* **2006**, *110*, 16482.
(44) Angelome, P. C.; Andrini, L.; Calvo, M. E.; Requejo, F. G.; Bilmes, S. A.; Soler-Illia, G. *J. Phys. Chem. C* **2007**, *111*, 10886.
(45) Notestein, J. M.; Andrini, L. R.; Kalchenko, V. I.; Requejo, F. G.; Katz, A.; Iglesia, E. *J. Am. Chem. Soc.* **2007**, *129*, 1122.
(46) Wu, Z. Y.; Ouvrard, G.; Gressier, P.; Natoli, C. R. *Phys. Rev. B* **1997**, *55*, 10382.
(47) Koudriachova, M. V.; Harrison, N. M.; de Leeuw, S. W. *Phys. Rev. Lett.* **2001**, *86*, 1275.
(48) Hewston, T. A.; Chamberland, B. L. *J. Phys. Chem. Solids* **1987**, *48*, 97.
(49) Borghols, W. J. H.; Lützenkirchen-Hecht, D.; Haake, U.; van Eck, E. R. H.; Mulder, F. M.; Wagemaker, M. *Phys. Chem. Chem. Phys.* **2009**, *11*, 5742.

JP908786T